The effects of heat and mass diffusion on freely oscillating bubbles in a viscoelastic, tissue-like medium

Carlos Barajas[a)] and Eric Johnsen

Mechanical Engineering Department, University of Michigan, Ann Arbor, Michigan 48109, USA

In certain cavitation-based ultrasound techniques, the relative importance of thermally vs mechanically induced damage is unclear. As a first step to investigate this matter, a numerical model for bubble dynamics in tissue-like, viscoelastic media is presented in which full thermal effects are included inside and outside the bubble, as well as interdiffusion of vapor and non-condensible gas inside the bubble. Soft tissue is assumed to behave according to a Kelvin-Voigt model in which viscous and elastic contributions are additive. A neo-Hookean formulation, appropriate for finite-strain elasticity, accounts for the large deformations produced by cavitation. Numerical solutions to problems of relevance to therapeutic ultrasound are examined, and linear analysis is used to explain the underlying mechanisms. The dependence between the surrounding medium's elasticity (shear modulus) and the extent to which the effects of heat and mass transfer influence bubble dynamics is quantified. In particular, the oscillation properties are related to the eigenvalues determined from linear theory. Regimes under which a polytropic relation describes the heat transfer to sufficient accuracy are identified, for which the complexity and computational expense associated with solving full partial differential equations can be avoided. © 2017 Acoustical Society of America.
[http://dx.doi.org/10.1121/1.4976081]

I. INTRODUCTION

While the primary motivation for cavitation research originally lay in hydrodynamics,[1,2] recent advances in ultrasound techniques, both diagnostic and therapeutic, have given rise to increased interest in acoustic cavitation.[3,4] For instance, encapsulated microbubbles can serve to improve contrast in ultrasound imaging or deliver drugs,[5] and several focused ultrasound techniques for therapy rely on cavitation, such as shock-wave lithotripsy,[6] high-intensity focused ultrasound (HIFU),[7] and histotripsy.[8] Bioeffects are common outcomes in these applications,[9,10] whether desired or not. One particular question related to bioeffects motivates the present study, namely, the relative importance of mechanically vs thermally induced damage in therapeutic ultrasound, specifically in HIFU and histotripsy.[11]

Analysis and modeling of cavitation dynamics are commonly conducted using the Rayleigh-Plesset equation,[12,13] a nonlinear ordinary differential equation (ODE) describing the response of a spherical gas or vapor bubble subjected to a far-field pressure change. Viscous, surface tension and compressibility effects can readily be included, and thermal transport has been investigated in the context of cavitation dynamics in water.[14] To improve the fidelity beyond a polytropic description of the gas inside the bubble, an energy equation can be solved inside the bubble to more accurately represent the thin thermal boundary layers[15] under the cold liquid assumption. More sophisticated approaches have been developed to account for the varying temperature in the surroundings as well.[16,17]

Mass transfer may be of importance in therapeutic ultrasound due to high tensions and multiple cycles. This topic has been the subject of several investigations. The conventional description of gases inside the bubble assumes that the contents include both vapor, which may condense, and non-condensible gas obeying a polytropic relation.[18] Most commonly, the vapor pressure is taken to be constant under thermodynamic equilibrium,[14] i.e., phase change is instantaneous and therefore does not affect the dynamics. Several studies have incorporated finite evaporation rates and other non-equilibrium effects.[19–23] Another aspect related to mass transfer is the diffusion of vapor and non-condensible gas in the bubble. Generally, the non-condensible gas is assumed insoluble,[24] which appears to be a reasonable assumption.[25] Based on the understanding thereby gathered, reduced-order models[22–24,26] were developed to decrease the cost and complexity of solving partial differential equations (PDEs) for heat and mass transfer, and were used to solve various bubble dynamics problems.[27,28] Such models have been used to investigate bubble dynamics in the context of therapeutic ultrasound,[22,23] although the surrounding medium was taken to be water.

One of the chief difficulties in modeling cavitation in ultrasound applications lies in representing the rheology of soft tissue, whose complex microstructure gives rise to a viscoelastic response. Assuming the bubble oscillates in a homogeneous medium, pioneering studies of cavitation in viscoelastic fluids motivated by polymer processing focused on Maxwell and Oldroyd constitutive models,[29–31] which introduce stress relaxation but do not enforce that the medium returns to its original configuration. These models were subsequently used to investigate cavitation in tissue.[32–35] More recently, it was recognized that models incorporating elasticity may represent soft

a)Electronic mail: carlobar@umich.edu

tissue more accurately since they preserve the original configuration after deformation. Examples include the Kelvin-Voigt models of Yang and Church,[36] strictly valid only for infinitesimal deformations, and of Gaudron *et al.*,[37] based on finite-strain theory and thus capable of representing large deformations, as well as the Zener models of Hua and Johnsen[38] and Warnez and Johnsen,[39] which in addition include relaxation. Although only one such model incorporates heat transfer,[39] no systematic study has been performed to determine how heat (and mass) transfer influences the bubble dynamics in visco-elastic media.

Quantifying mechanical vs thermal effects of bubbles on soft tissue requires an accurate representation of the mechanics and heat transfer. At the present time, the effects of heat and mass transport on bubbles oscillating in soft materials, with application to therapeutic ultrasound, is unknown. Our objective is to address this knowledge gap. In particular, we use a numerical model for spherical bubble dynamics to represent a freely oscillating bubble under circumstances of relevance to therapeutic ultrasound in a viscoelastic medium representative of soft tissue. To elucidate the underlying mechanisms, we theoretically and numerically investigate the bubble oscillation properties. The key novelty of this work lies in the inclusion of elasticity in investigations of heat and mass transfer in bubble dynamics, both numerical and analytical. The article is laid out as follow. First, we describe our physical and numerical models, as well as our linear analysis approach. We then present numerical results and explain them with the help of the linear analysis. We close by summarizing our findings and discussing future research directions.

II. PHYSICAL MODEL

A. Equations of motion

We consider the spherical dynamics of a bubble in an infinite viscoelastic medium. Taking into account acoustic radiation losses due to the compressibility of the medium, the bubble dynamics are represented by the Keller-Miksis ODE[40]

$$
\left(1 - \frac{\dot{R}}{c}\right) R\ddot{R} + \frac{3}{2}\left(1 - \frac{\dot{R}}{3c}\right)\dot{R}^2
$$
$$
= \left(1 + \frac{\dot{R}}{c} + \frac{R}{c}\frac{d}{dt}\right)\frac{p - p_\infty(t) - \Theta_{\mathrm{ve}} - \frac{2S}{R}}{\rho}, \tag{1}
$$

where R is the bubble radius, ρ and c are the density and sound speed of the surroundings, S the surface tension, p the internal bubble pressure given by the sum of the partial pressures of non-condensible gas (p_g) and vapor (p_v), Θ_{ve} is the viscoelastic stress integral, and $p_\infty(t)$ is the far-field driving pressure. The overdots denote derivatives with respect to time t.

The approach of Gaudron *et al.*[37] is followed to represent the soft tissue's finite deformations created by large-amplitude bubble oscillations of interest in the problems of interest (from 10% to over 200% strains), and the corresponding stresses described by nonlinear elastic theory, by

contrast to infinitesimal strains and linear elastic theory. The integral of the total stress is the sum of viscous and elastic contributions

$$
\Theta_{\mathrm{ve}} = \frac{4\mu\dot{R}}{R} + \frac{G}{2}\left[5 - 4\frac{R_{\mathrm{sf}}}{R} - \left(\frac{R_{\mathrm{sf}}}{R}\right)^4\right], \tag{2}
$$

where μ is the viscosity of the surroundings, G is the (linear) shear modulus, and R_{sf} is the bubble radius corresponding to stress-free surroundings; depending on the problem under consideration, R_{sf} may be the initial radius R_o or the equilibrium radius R_e. This Kelvin-Voigt formulation implies that the surrounding medium possesses an original configuration, which is an attribute of most soft tissues. Given the large deformations of the surroundings, the elastic stress is computed based on a neo-Hookean constitutive relation, which accounts for finite-strain (nonlinear) elasticity. In the surrounding medium, the rr- and $\theta\theta$-components of the elastic stress tensor are given by

$$
\tau_{rr} = \frac{2}{3}G\left[\left(\frac{r_o}{r}\right)^4 - \left(\frac{r}{r_o}\right)^2\right], \quad \tau_{\theta\theta} = -\frac{1}{2}\tau_{rr}, \tag{3}
$$

where $r_o(r, t) = (r^3 - R^3 + R_{\mathrm{sf}}^3)^{1/3}$ is the radial location in the original configuration.

The bubble is assumed homobaric. Heat and mass transfer both modify the bubble pressure evolution[41]

$$
\dot{p} = \frac{3}{R}\left[-\gamma p\dot{R} + (\gamma - 1)K_w\frac{\partial T}{\partial r}\big|_w + \gamma\mathcal{R}_v T_w\dot{m}_v''\right], \tag{4}
$$

where $T(r, t)$ is the instantaneous, spatially varying temperature, K is the mixture thermal conductivity inside the bubble, $\mathcal{R}_v$ is the gas constant of vapor, and $\dot{m}_v''$ the vapor mass flux across the interface. The subscript w denotes variables evaluated at the bubble wall. The specific heats ratio γ of vapor is assumed equal to that of air.

To account for heat transfer, we compute PDEs for energy balance inside and outside the bubble, with Fourier's law to describe heat conduction. Inside the bubble,

$$
\frac{\gamma}{\gamma - 1}\frac{p}{T}\left(\frac{\partial T}{\partial t} + U\frac{\partial T}{\partial r}\right) - \dot{p} = [\nabla \cdot (K\nabla T)]_r, \tag{5}
$$

where only the radial terms are non-zero (denoted by the r subscripts) and

$$
U = \frac{1}{\gamma p}\left[(\gamma - 1)K\frac{\partial T}{\partial r} - \frac{r\dot{p}}{3}\right]. \tag{6}
$$

The mixture thermal conductivity is given by $K = AT + B$, where A and B are experimentally determined coefficients.[15]

Outside the bubble,

$$
\frac{\partial T_s}{\partial t} + \frac{R^2\dot{R}}{r^2}\frac{\partial T_s}{\partial r} = D_s\left[\nabla^2 T_s\right]_r + \frac{12\mu}{\rho C_p}\left(\frac{R^2\dot{R}}{r^3}\right)^2, \tag{7}
$$

where T_s is the temperature in the surroundings, C_p is the heat capacity at constant pressure, $D_s = K_s/(\rho C_p)$ is the thermal diffusivity, and K_s is the constant thermal conductivity of the surroundings.

Carlos Barajas and Eric Johnsen   909

The boundary conditions imposed on Eqs. (5) and (7) are, for the temperature,

$$T_w = T_{s,w}, \quad T_s|_{r\to\infty} \to T_\infty, \tag{8}$$

and for the fluxes,

$$\left.\frac{\partial T}{\partial r}\right|_{r=0} = 0, \quad L\dot{m}_v'' = K_s \left.\frac{\partial T_s}{\partial r}\right|_w - K\left.\frac{\partial T}{\partial r}\right|_w, \tag{9}$$

where T_∞ is the far-field temperature and L is the latent heat of condensation/evaporation. Thus, the energy formulation includes energy transfer due to phase change.

With regard to mass transfer, equilibrium phase change is considered at the bubble wall, the interdiffusion of non-condensible gas and vapor are computed inside the bubble; it is assumed that no transfer of non-condensible gas takes place from the surroundings into the bubble, e.g., rectified diffusion.[42] This assumption is valid due to the low solubility of air in water ($C_g \sim 10^{-5}$) and the short time scales associated with the bubble oscillations, compared to those of rectified diffusion.[24] Thus, the main challenge lies in determining the vapor (alternately, the non-condensible gas) concentration inside the bubble. Mass diffusion is represented by Fick's law such that the mass balance equation for vapor reads[21]

$$\frac{\partial C}{\partial t} + u\frac{\partial C}{\partial r} = \frac{[\nabla \cdot (D\rho_m \nabla C)]_r}{\rho_m}, \tag{10}$$

where

$$u = U + \frac{\mathcal{R}_v - \mathcal{R}_g}{\mathcal{R}}\frac{\partial C}{\partial r}, \tag{11}$$

$C = \rho_v/\rho_m$ is the vapor mass concentration, ρ_v is the vapor density, ρ_m is the mixture density, D is the diffusion coefficient between water vapor and air, $\mathcal{R}_g$ is the gas constant of air, and $\mathcal{R} = C\mathcal{R}_v + (1 - C)\mathcal{R}_g$ is the mixture gas constant. The boundary conditions are

$$\left.\frac{\partial C}{\partial r}\right|_{r=0} = 0, \quad \rho_w C_w = \frac{p_{v,sat}(T_w)}{\mathcal{R}_v T_w}, \tag{12}$$

with the latter equality arising from assuming equilibrium phase change. The saturated vapor pressure at the bubble wall is given by

$$p_{v,sat}(T_w) = p_{ref}\,\exp\left(-\frac{T_{ref}}{T_w}\right), \tag{13}$$

where p_{ref} and T_{ref} are empirically determined parameters.[24] In tissue, phase change is expected to be inhibited by the constraining effect of tissue on water, the extent of which is presently unknown; Eq. (13) thus provides an upper limit for vaporization and condensation across the bubble wall, since it strictly applies to water. Assuming the mixture obeys the ideal gas law, C and ρ_m are related by

$$C = \frac{1}{\mathcal{R}_v - \mathcal{R}_g}\left(\frac{p}{\rho_m T} - \mathcal{R}_g\right). \tag{14}$$

Finally, the vapor mass flux is written

$$\dot{m}_v'' = D\frac{\rho_{m,w}}{1 - C_w}\left.\frac{\partial C}{\partial r}\right|_w. \tag{15}$$

Accurate measurement of the viscoelastic properties of soft materials at the rates of interest are challenging.[43] Table I lists the material properties used in this study, selected to be relevant in the context of therapeutic ultrasound.[36,38,39] Since soft tissue exhibits a range of stiffnesses,[44] an important goal of the present study is to describe different behaviors of the bubble dynamics as G is varied.

B. Non-dimensionalization and geometry

It is convenient to numerically solve the equations in dimensionless form. For non-dimensionalization, we use the initial bubble radius R_0, atmospheric pressure p_∞, the medium density ρ, and the far-field temperature T_∞; from these quantities, a characteristic velocity $U_C = \sqrt{p_\infty/\rho}$ is constructed. This gives rise to the following dimensionless parameters: Reynolds number $\mathrm{Re} = \rho U_c R_0/\mu$, Cauchy number $\mathrm{Ca} = P_\infty/G$, Weber number $\mathrm{We} = p_\infty R_0/2S$, mass Fourier number $\mathrm{Fo}_m = D/(U_c R_0)$, heat Fourier number $\mathrm{Fo}_h = D_s/(U_c R_0)$, Brinkman number $\mathrm{Br} = U_c^2/C_p T_\infty$, dimensionless sound speed $C = c/U_c$, and $\chi = T_\infty K_\infty/(p_\infty R_0 U_c)$. Time and frequency are non-dimensionalized by R_0/U_C. From here on, we refer to t as dimensionless time.

We transform the spherically symmetric domain with radial coordinate r into a new variable $y = r/R$. Outside the bubble, we further implement the following transformation, $x = 2/(1 + (y - 1)/L_t) - 1$, to set the integration limits to $x \in [1, -1]$. L_t is a scaling factor for the domain.[17] Finally, to simplify the energy Eq. (5) inside the bubble, we transform the temperature,

$$\theta = \frac{1}{K_\infty}\int_1^T K(T_\infty\theta')d\theta'. \tag{16}$$

As a result, we re-write the two nonlinear ODEs and three PDEs in dimensionless form

TABLE I. Baseline values for the material properties used in the present study.

Property	Nominal value	Property	Nominal value	Property	Nominal value
A	5.3×10^{-5} W/mK^2	S	5.6×10^{-2} N/m	C_p	4.18 kJ/kgK
B	1.17×10^{-2} W/mK	μ	15 cP	L	2.264×10^6 J/kg
D	24.2×10^{-6} m^2/s	p_∞	101.3 kPa	γ	1.4
K_l	0.55 W/m	T_∞	298.15 K	p_{ref}	1.17×10^8 kPa
T_{ref}	5200 K	ρ	1060 kg/m^3	c	1430 m/s

    Carlos Barajas and Eric Johnsen

$$\left(1 - \frac{\dot{R}}{C}\right) R\ddot{R} + \frac{3}{2}\left(1 - \frac{\dot{R}}{3C}\right)\dot{R}^2$$
$$= \left(1 + \frac{\dot{R}}{C} + \frac{R}{C}\frac{d}{dt}\right)\left[p - p_\infty(t) - \frac{4\dot{R}}{\mathrm{Re}R}\right.$$
$$\left. - \frac{1}{\mathrm{We}R} - \frac{1}{2\mathrm{Ca}}\left(5 - \frac{4R_{sf}}{R} - \frac{R_{sf}^4}{R^4}\right)\right], \tag{17}$$

$$\dot{p} = \frac{3}{R}\left[-\gamma p\dot{R} + \frac{(\gamma-1)\chi}{R}\frac{\partial\theta}{\partial y}\bigg|_w + \frac{\gamma\mathcal{R}_v\mathrm{Fo}_m p}{T_w R(1-C_w)\mathcal{R}_w}\frac{\partial C}{\partial y}\bigg|_w\right], \tag{18}$$

$$\frac{\gamma}{\gamma-1}\frac{p}{TK}\left(\frac{\partial\theta}{\partial t} + \frac{U - y\dot{R}}{R}\frac{\partial\theta}{\partial y}\right) - \dot{p} = \frac{\chi}{R^2}[\nabla^2\theta]_y, \tag{19}$$

$$\frac{\partial C}{\partial t} + \frac{u - y\dot{R}}{R}\frac{\partial C}{\partial y} = \frac{\mathrm{Fo}_m}{R^2}\frac{[\nabla\cdot(\rho_m\nabla C)]_y}{\rho_m}, \tag{20}$$

$$\frac{\partial T_s}{\partial t} = \frac{(1+x)^2}{L_t R}\left[\frac{\mathrm{Fo}_h}{R}\left(\frac{1+x}{2L_t} - \frac{1}{y}\right) + \frac{\dot{R}}{2}\frac{1-y^3}{y^2}\right]\frac{\partial T_s}{\partial x}$$
$$+ \frac{\mathrm{Fo}_h}{4}\frac{(1+x)^4}{L_t^2 R^2}\frac{\partial^2 T_s}{\partial x^2} + 12\frac{\mathrm{Br}}{\mathrm{Re}}\frac{\dot{R}^2}{R^2 y^6}, \tag{21}$$

with

$$U = \frac{1}{\gamma p}\left[\frac{(\gamma-1)\chi}{R}\frac{\partial\theta}{\partial y} - \frac{yR\dot{p}}{3}\right], \tag{22}$$

$$u = U + \frac{\mathrm{Fo}_m}{R}\frac{\mathcal{R}_v - \mathcal{R}_g}{\mathcal{R}}\frac{\partial C}{\partial y}. \tag{23}$$

III. NUMERICAL METHOD

A fifth-order explicit Dormand-Prince Runge-Kutta method[45] with adaptive stepsize control is used to march the ODEs and PDEs forward in time. At each substep, the PDEs are discretized using $N_y + 1$ equidistant points in y-space inside the bubble and solved using second-order central differences following directly,[15] e.g., for the concentration

$$\frac{\partial C}{\partial y}\bigg|_{y=i} \approx \frac{C_{i+1} - C_{i-1}}{2\Delta y}, \tag{24}$$

$$\nabla^2 C|_{y=i} \approx \frac{\left(1 + \frac{\Delta Y}{y_{i+1}}\right)C_{i+1} - 2C_i + \left(1 - \frac{\Delta Y}{y_{i-1}}\right)C_{i-1}}{\Delta y^2}, \tag{25}$$

where $\Delta y = 1/N_y$ and $y_i = (i-1)/\Delta y$. A second-order one-sided difference is used at the bubble wall. The same discretization is used for the temperature. Outside the bubble, the energy equation is treated in a similar manner, by discretizing x-space with $N_x + 1$ equidistant points. All simulations were carried out with $N_x = N_y = 1000$. The treatment of the interface conditions deserves additional explanations. Expanding the finite difference expressions at the boundary results in an algebraic expression for T_w, which is solved

using an algorithm based on a combination of bisection, secant, and inverse quadratic interpolation.[46] The convergence of the overall method is evaluated in Appendix A 1.

IV. LINEAR ANALYSIS

We use linear analysis to explain the contributions of heat and mass transfer on the bubble dynamics. For simplicity, we use reduced-order models[24] to describe the heat and mass transfer at the bubble wall,

$$\frac{\partial C}{\partial y}\bigg|_w \cong -\beta_C(\bar{C} - C_w), \quad \frac{\partial T}{\partial y}\bigg|_w \cong -\beta_T(\bar{T} - T_w), \tag{26}$$

where $\bar{C}$ and $\bar{T}$ are the volume-averaged concentration and temperature, respectively,

$$\bar{C} = \frac{m_v}{m_v + m_{g0}}, \quad \bar{T} = \frac{p}{p_0}R^3\frac{\mathcal{R}_v m_{v0} + \mathcal{R}_g m_{g0}}{\mathcal{R}_v m_v + \mathcal{R}_g m_{g0}}. \tag{27}$$

The expression for the volume averaged temperature differs from that in Ref. 24 in that we take into consideration the dependence of $\mathcal{R}$ on concentration.

The mass of non-condensible gas inside the bubble m_{g0} is constant, while the mass of vapor in the bubble m_v is obtained by assuming equilibrium phase change,

$$\frac{dm_v}{dt} = 4\pi R^2\dot{m}_v''. \tag{28}$$

The coefficients β_l in Eq. (26) are given by[24]

$$\beta_l(J) = \Re\left(\left[\sqrt{J}\coth\sqrt{J}\right]^{-1} - \frac{3}{J}\right)^{-1}, \tag{29}$$

where $J = i\omega_N/l$, $l = \chi$ for mass transfer and $l = \mathrm{Fo}_m$ for heat transfer, and the isothermal bubble natural frequency $\omega_N = \sqrt{3(p_\infty - p_v) + 2/\mathrm{We} + 4/\mathrm{Ca}}$. Thus, in the analysis, Eqs. (19), (20), and (21) are no longer solved. Instead, we end up with a 4×4 system of first-order nonlinear ODEs,

$$\frac{d}{dt}\mathbf{X} = \mathbf{F}, \quad \mathbf{X} = (R, \dot{R}, p, m_v)^T, \tag{30}$$

where $\mathbf{F}(\mathbf{X}) = (f_1(\mathbf{X}), f_2(\mathbf{X}), f_3(\mathbf{X}), f_4(\mathbf{X}))$ is defined via Eqs. (17), (18), and (28). This system of equations is linearized about its fixed points $\mathbf{X}_e$, yielding

$$\frac{d}{dt}\tilde{\mathbf{X}} = \mathbf{A}\tilde{\mathbf{X}}, \quad A_{ij} = \frac{\partial F_i}{\partial X_j}\bigg|_{\mathbf{X}_e}, \tag{31}$$

where $\tilde{\mathbf{X}} = \mathbf{X} - \mathbf{X}_e$ for small perturbations from $\mathbf{X}_e$, and the Jacobian matrix A_{ij} is evaluated at the fixed points given by the following algebraic system of equations:

$$p_e - (1+f) = \frac{1}{\mathrm{We}R_e} + \frac{1}{2\mathrm{Ca}}\left(5 - \frac{4R_{sf}}{R_e} - \frac{R_{sf}^4}{R_e^4}\right), \tag{32}$$

$$\dot{R}_e = 0, \tag{33}$$

$$\frac{p_e}{p_0} R_e^3 \frac{\mathcal{R}_v m_{v0} + \mathcal{R}_g m_{g0}}{\mathcal{R}_v m_{ve} + \mathcal{R}_g m_{g0}} = 1, \tag{34}$$

$$\frac{m_{ve}}{m_{v0} + m_{g0}} = \frac{1}{1 + \frac{\mathcal{R}_v}{\mathcal{R}_g} \left[\frac{p_e}{p_{v,\text{sat}}(T_w)} - 1 \right]}. \tag{35}$$

The subscript e indicates equilibrium conditions (fixed points). For harmonic forcing $f = 0$, and for Rayleigh collapse $f = \Delta p$.

The four eigenvalue and eigenvector pairs of $\mathbf{A}$, $(\lambda_1, \mathbf{v}_1), (\lambda_2, \mathbf{v}_2), (\lambda_3, \mathbf{v}_3)$, and $(\lambda_4, \mathbf{v}_4)$, can be numerically computed, with

$$\tilde{\mathbf{X}} = \sum_{i=1}^{4} c_i \mathbf{v_i} e^{\lambda_i t}, \quad \mathbf{C} = \mathbf{V}^{-1} \tilde{\mathbf{X}}_o, \tag{36}$$

where $\mathbf{C} = (c_1, c_2, c_3, c_4)^T$ and $\mathbf{V} = (\mathbf{v}_1, \mathbf{v}_2, \mathbf{v}_3, \mathbf{v}_4)$. The bubble radius is then $R(t) \approx R_e + \tilde{X}_1(t)$. By considering the eigenvalue (λ_{dom}) that dominates $X_1(t)$, the damped natural frequency ω_d and the time constant t_d can be calculated:

$$\omega_d = \Im(\lambda_{dom}), \quad t_d = \frac{-1}{\Re(\lambda_{dom})}. \tag{37}$$

We demonstrate in Appendix A 2 that the linear analysis displays good agreement with our numerical results for sufficiently low-amplitude oscillations.

V. RESULTS AND DISCUSSION

To illustrate the salient features of heat and mass transfer on free oscillations of a bubble in tissue-like media, two forms of bubble collapse problems[37,39] are solved, driven by pressure ratios of relevance to therapeutic ultrasound, and three different approaches are evaluated: polytropic (adiabatic), heat transfer only, and heat and mass transfer (full model). To facilitate comparisons with the linear analysis, the present Keller-Miksis simulations are run with the heat and mass transfer models of Ref. 24 including the cold water assumption, except at the very end of each section where the temperature field is shown.

A. Step increase in surrounding pressure (classical Rayleigh collapse)

We first consider the classical Rayleigh collapse problem[12] wherein the bubble, initially in equilibrium with its surroundings, undergoes collapse due to the instantaneous increase in the far-field pressure ($\Delta p = 35 p_\infty$). This pressure increase causes the bubble to collapse and oscillate to a new equilibrium radius. Initially the medium is stress free ($R_{sf} = R_o$) and the pressure inside the bubble is given by $p_o = p_\infty + 1/(\text{We} R_o)$, unless otherwise mentioned. The initial radius is 3 μm and the initial velocity is $\Delta p/(\rho c)$.[14] We first recall the results of Ref. 38, and consider in Fig. 1 the time evolution of the bubble radius for different shear moduli using the polytropic model. Note that the initial bubble radii considered in that study was $R_o = 5 \mu$m. As the shear modulus is increased (decreasing Cauchy number), the
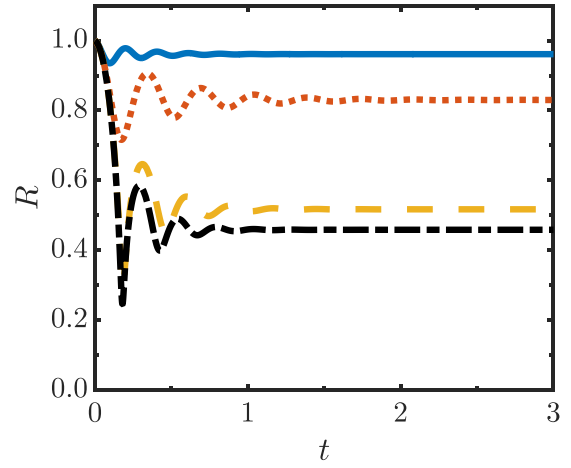

FIG. 1. (Color online) Time evolution of the bubble radius for different shear moduli for classical Rayleigh collapse using the polytropic model ($\Delta p = 35 p_\infty$, $R_o = 5 \mu$m). Ca = 0.005 (solid blue), 0.030 (dotted red), 0.600 (dashed orange), and 1000 (dashed-dotted black). Results presented in dimensionless form.

equilibrium radius becomes larger since the final state of stress increases accordingly. Starting from the lowest shear modulus, the persistence of the oscillations first increases as the Cauchy number is decreased, and then decreases for $0.030 \lesssim \text{Ca} \lesssim 0.005$; in other words, the damping decreases with increasing Ca, reaches a minimum between 0.030 and 0.005, and increases again thereafter. For this problem, the solution with Ca = 1000 is nearly identical to that of a Newtonian liquid.

The effects of heat and mass transfer as a function of elasticity are assessed in Fig. 2. For the larger Cauchy numbers (Ca = 0.6, 1000), i.e., lower shear moduli, the equilibrium radius and oscillation properties of the solution with thermal effects exhibit clear discrepancies from the polytropic case: the equilibrium radius is smaller, and the oscillations die out sooner, thus suggesting increased damping. An illustration of the complexity of the high-order system is discerned in the Ca = 1000 case: in addition to "conventional" damping observed in the peak-to-peak decrease of the rebounds, the full model exhibits an additional, slower, over-damped time scale visible in the non-zero slope between 1.0 and 2.0. For these parameters, mass transfer inside the bubble does not visibly affect the results, i.e., vapor trapping[20] is negligible because the vapor pressure is far smaller than the gas pressure.

Small-amplitude (linear) perturbation analysis can be used to investigate the behavior observed above. We consider the dependence of the equilibrium radius, time constant, and damped natural frequency on the Cauchy number in Fig. 3. The polytropic results are consistent with those observed in past studies.[38] As the Cauchy number is increased (shear modulus decreased), the equilibrium radius becomes smaller due to the reduced final stress state; the same non-monotonic behavior of the time constant and damped natural frequency as a function of Cauchy number is observed. At low Ca (high shear modulus), the oscillation amplitude is small such that the bubble temperature never reaches sufficiently high values for substantial heat transfer;

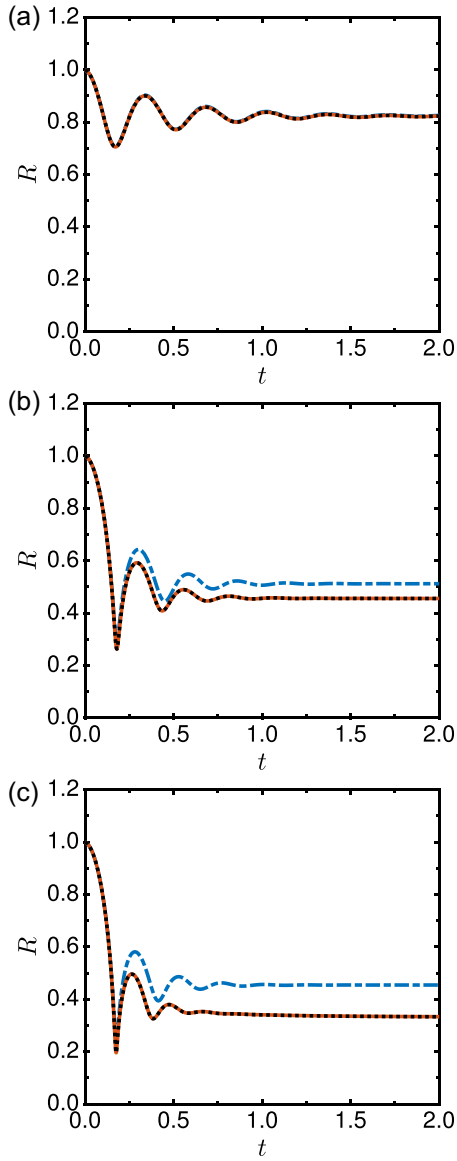Carlos Barajas and Eric Johnsen

FIG. 2. (Color online) Time evolution of the bubble radius for different shear moduli for classical Rayleigh collapse using the polytropic (dashed-dotted blue), heat transfer only (solid red), heat/mass transfer (dotted black) models ($\Delta p = 35 p_\infty$, $R_o = 3 \ \mu$m). Ca = 0.03 (top), 0.60 (middle), 1000 (bottom). Results presented in dimensionless form.
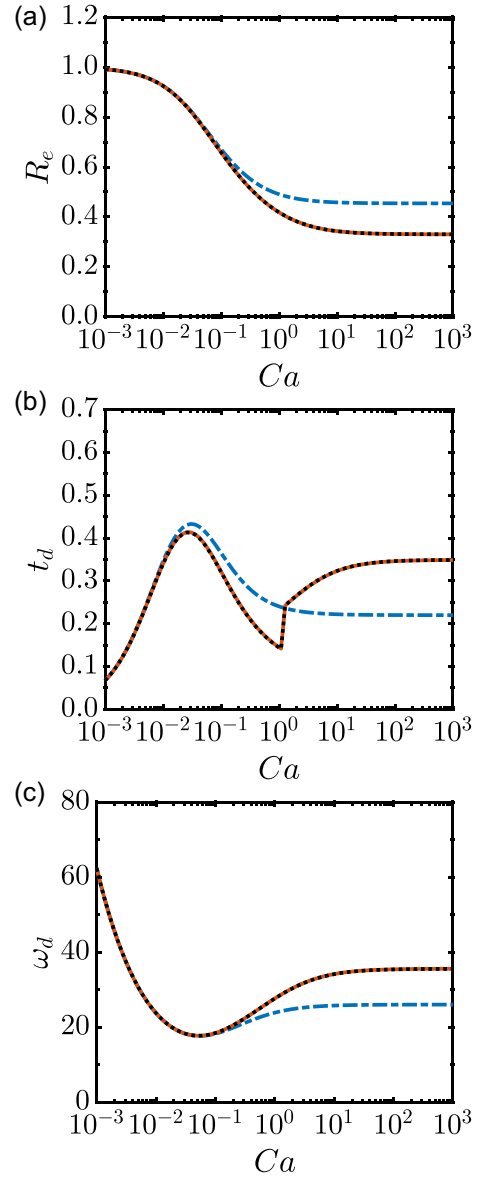

FIG. 3. (Color online) Dependence of the equilibrium radius (top), time constant (middle), and damped natural frequency (bottom) on the Cauchy number for classical Rayleigh collapse based on linear analysis using the polytropic (dashed-dotted blue), heat transfer only (solid red), and heat/mass transfer (dotted black) models ($\Delta p = 35 p_\infty$, $R_o = 3 \ \mu$m). Results presented in dimensionless form.

the full model agrees with the polytropic solution. At Ca $\gtrsim 0.1$, the equilibrium radius when including heat transfer starts to diverge from the adiabatic solution. The oscillation amplitude is larger, leading to higher collapse temperatures and thus non-negligible heat transfer. For Ca = 0.60 and 1000, the discrepancy in the equilibrium radius between the polytropic solution and that including heat (and mass) transfer is due to the fact that no heat transfer takes place in the polytropic (adiabatic) case. Thus, the equilibrium temperature need not relax to the temperature of the surroundings at late times and in fact remains higher since no heat is lost. When accounting for heat transfer, the equilibrium temperature eventually ends up equal to the ambient temperature, as expected.

The time constant, determined by considering the real part of the dominant eigenvalue, exhibits a complicated

dependence on Cauchy number when accounting for heat transfer. Since the polytropic model includes only compressible and viscous damping and since the corresponding characteristic polynomial only has two roots, the interpretation is straightforward:[38] compressible damping is dominant at low Cauchy number and decreases with increasing Ca, while viscous damping follows the opposite behavior; thus, the addition of the viscous and compressible damping contributions gives rise to a non-monotonic behavior. Thermal damping can be inferred by comparing the results with heat transfer to the polytropic case. At low Ca, there is little difference with the polytropic case; thermal damping is negligible and compressible damping dominates, as in Ref. 38. For 0.01 $\lesssim$ Ca $\lesssim O(1)$, the time constant follows a trend similar to that of the polytropic case, but with a lower value. We thus

infer that in this range of shear modulus thermal damping is important, but does not significantly change the dynamics. At Ca $\approx$ 1, there is a sudden increase in the time constant beyond the corresponding polytropic value, after which the time constant tends to an asymptotic value of $\sim$0.35 (by contrast to 0.22 in the polytropic case). This behavior indicates that thermal damping becomes important for Ca $\gtrsim$ 1. In the presence of heat transfer, the damped natural frequency is almost identical to the polytropic case at low Cauchy number. At Ca $\approx O(1)$, thermal effects give rise to a high frequency and thus shorter oscillation period observed in Fig. 2 compared to the polytropic solution. Unlike the behavior of the time constant, no drastic change is observed in ω_d at Ca $\sim O(1)$.

Additional insight is gained by mapping the eigenvalues of the system for different shear moduli in Fig. 4. When thermal effects are included, the governing system is third order, so a third eigenvalue exists (and a fourth when mass transfer is included). In the full model, there are two real and two imaginary eigenvalues for the parameters of interest. The corresponding polytropic equation system has only two poles, which are complex as long as the system is not overdamped. At the lowest elasticity (Ca = 1000), the pair of complex eigenvalues dominate the system as illustrated by the persistence of oscillations; the right-most purely real eigenvalue governs a second, exponential decaying time scale observable in the oscillations shown in Fig. 2 (bottom). As the Cauchy number is decreased, the right-most real eigenvalue moves to the left while the pair of complex eigenvalues move to the right; at some Cauchy number between 0.03 and 0.60, the complex eigenvalues "overtake" the right-most purely real eigenvalue—their real part is farther to the right, thus, explaining the sharp increase in the time constant (Fig. 3, middle). At the highest elasticity (Ca = 0.03) the system is dominated by the two complex poles; the relative magnitude of the purely real eigenvalues makes them irrelevant.

However, the dynamics are not completely governed by the dominant eigenvalues; one must also consider the initial conditions and account for the contributions of all eigenvalues.

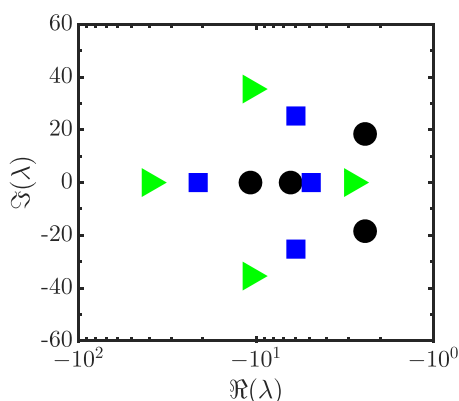Given the computational expense incurred to model heat/mass transfer, it is of practical interest to know whether the full PDEs must be solved. Overall, the linear analysis and simulations indicate that the effects of heat (and mass) transfer are negligible for Ca $\lesssim$ 0.03, given this value of Δp. Since most soft tissues are in the 1–100 kPa range—well within the 3.4 MPa corresponding to Ca = 0.03, the full system should be solved.

The simulations for this problem setup were executed using the cold liquid assumption to allow a direct comparison to the linear results. This assumption can be relaxed to calculate the temperature field in the surroundings, as shown in Fig. 5. The bubble dynamics are nearly identical to those obtained with the cold liquid simulation. For this problem, a particle in the surrounding medium very near the bubble wall experiences a temperature rise of approximately 45 °C during the first collapse.

B. Step decrease in internal pressure ("Flynn collapse")

The alternate bubble collapse problem wherein the surrounding pressure is kept constant but the internal pressure is reduced is considered next. This problem, particularly relevant to cavitation bubble growth and collapse in ultrasound- and laser-induced cavitation, was studied in detail by Flynn;[47,48] for conciseness, we refer to this problem as "Flynn collapse." Reducing the internal pressure corresponds to starting the problem with an initial radius larger than the equilibrium radius. To facilitate comparisons, we consider the bubble to be in a stress-free state at equilibrium ($R_{sf} = R_e$); in practice (e.g., laser cavitation), the equilibrium radius is larger than the nucleus size, such that the bubble is not in a stress-free state at equilibrium.

The initial bubble pressure is $p_o = p_v + p_a$, where $p_v = p_{v,sat}(T_\infty) = 3.09$ kPa and $p_a = 8$ kPa; this corresponds to a pressure ratio driving the collapse of 8.5. As the shear modulus is increased, an additional elastic stress acts on the bubble. The initial radius $R_o = 3$ μm is 2.09 times greater than the equilibrium radius for the polytropic model; when accounting for full thermal effects, $R_o/R_e = 2.97$ for this pressure ratio. The initial velocity is $\Delta p_o/(\rho c)$.[14] In Fig. 6,
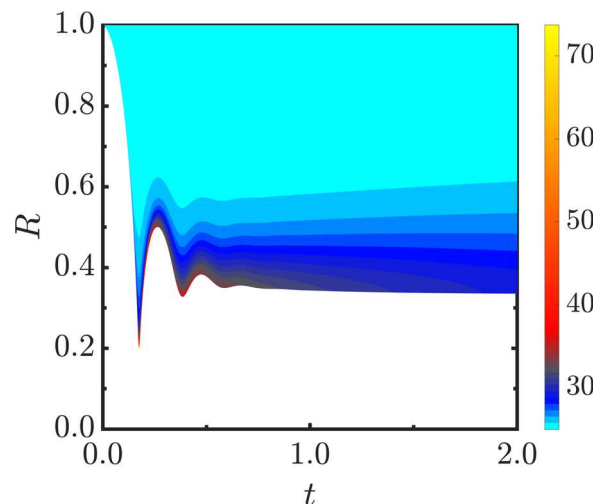

FIG. 4. (Color online) Eigenvalue map for classical Rayleigh collapse ($\Delta p = 35 p_\infty$, $R_o = 3$ μm), with Ca = 0.03 (black circle), 0.60 (blue square), and 1000 (green triangle). Results presented in dimensionless form.

FIG. 5. (Color online) Temperature distribution in the surroundings for classical Rayleigh collapse ($\Delta p = 35 p_\infty$, $R_o = 3$ μm, Ca = 1000). Results presented in dimensionless form except for temperature (degrees Celsius).

Carlos Barajas and Eric Johnsen

we examine the time evolution of the bubble radius for different shear moduli using the polytropic model. At the highest Cauchy number, the damping is near critical. As the Cauchy number is decreased (shear modulus increased), the oscillation amplitude increases. Although seemingly counter-intuitive, this behavior is explained by considering the state of stress at $t = 0$, which increases as the shear modulus is increased, thus, leading to more violent collapse.

The dependence of heat and mass transfer effects on elasticity is assessed in Fig. 7. As the Cauchy number is increased (shear modulus is reduced), the oscillations become overdamped. By contrast to the results in Sec. IV, the polytropic solution never agrees with the solution with heat transfer: the equilibrium radius in Eq. (32) does not change as the shear modulus is varied, as expected since the equilibrium conditions are the same in all cases. Again, the equilibrium radius is larger for the polytropic case, since heat is not dissipated. For these parameters, mass transfer inside the bubble again does not visibly affect the results.

As in Sec. IV, linear analysis is invoked to explain the results. We consider the dependence of the time constant and damped natural frequency on the Cauchy number in Fig. 8. In the polytropic case, the time constant increases rapidly with Cauchy number before reaching a plateau of ~ 2.4 at $\text{Ca} \approx O(1)$. When heat transfer is included, the growth at low Ca is slower than for the polytropic case and appears to reach a plateau; then, at $\text{Ca} \approx 1$ the regime changes. The damped natural frequency monotonically decreases with increasing Ca in the polytropic case. When heat transfer is included, ω_d starts from a higher value than the polytropic solution at low Cauchy numbers, decreases before crossing the polytropic solution at $\text{Ca} \approx 1$, and becomes zero at $\text{Ca} \gtrsim 1$, at which point the system is overdamped. It is thus clear that the change in regime in the time constant is due to the solution being overdamped beyond $\text{Ca} \sim O(1)$. These results explain the increased damping observed in Fig. 6 as the Cauchy number is increased.

The eigenvalue map (Fig. 9) confirms the results shown in Sec. V B. For the lowest Cauchy numbers, the system is dominated by a pair of complex poles, with two small, purely real poles. As Ca is increased, these poles move toward the real axis and reach it by $\text{Ca} = 10$. Beyond this
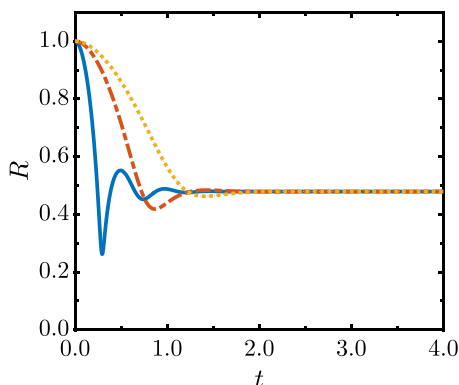

FIG. 6. (Color online) Time evolution of the bubble radius for different shear moduli for Flynn collapse using the polytropic model ($R_o/R_e = 2.09$). Ca $= 0.1$ (solid blue), 1.0 (dashede-dotted red), and 10 (dotted yellow). Results presented in dimensionless form.
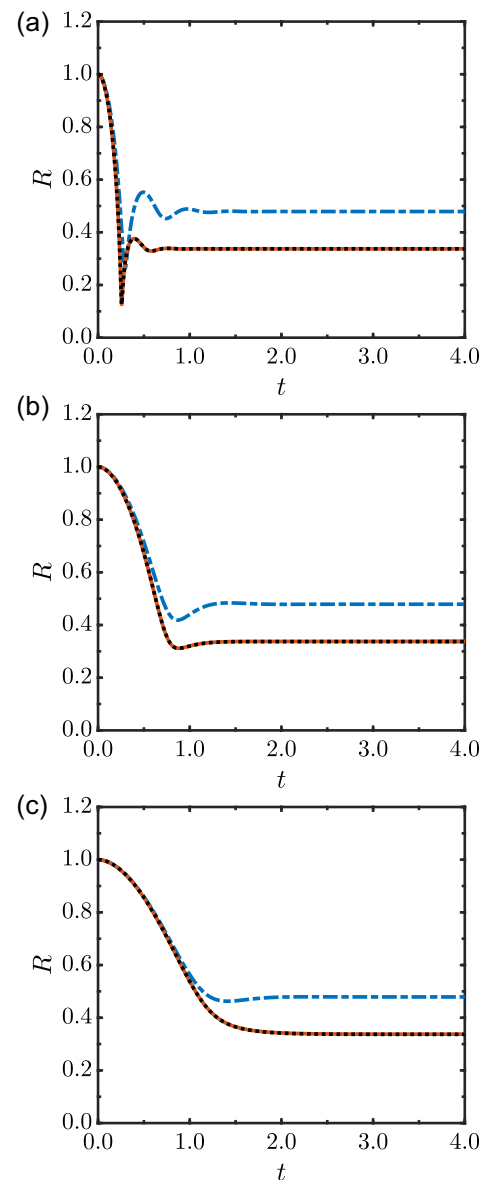

FIG. 7. (Color online) Time evolution of the bubble radius for different values of shear modulus for Flynn collapse using the polytropic (dashed-dotted blue), heat transfer only (solid red), and heat/mass transfer (dotted black) models ($R_o/R_e = 2.09$ for the polytropic model, $R_o/R_e = 2.97$ with full thermal effects). Ca $= 0.1$ (top), 1.0 (middle), and 10 (bottom). Results presented in dimensionless form.

Cauchy number, the oscillations are overdamped. The other two fast real poles do not change with elasticity.

As for the classical Rayleigh collapse problem, the cold liquid assumption is relaxed to determine the temperature field in the surroundings (Fig. 10). Again, due to the small radius at collapse, a particle in the surrounding medium very near the bubble wall experiences a temperature rise of $\sim 20\ ^\circ\text{C}$. The thermal boundary layer in the surroundings diffuses over time. The bubble dynamics are nearly identical to those obtained with the cold liquid assumption.

VI. CONCLUSIONS

In this study, free oscillations of a vapor bubble in tissue-like, viscoelastic media under conditions relevant to
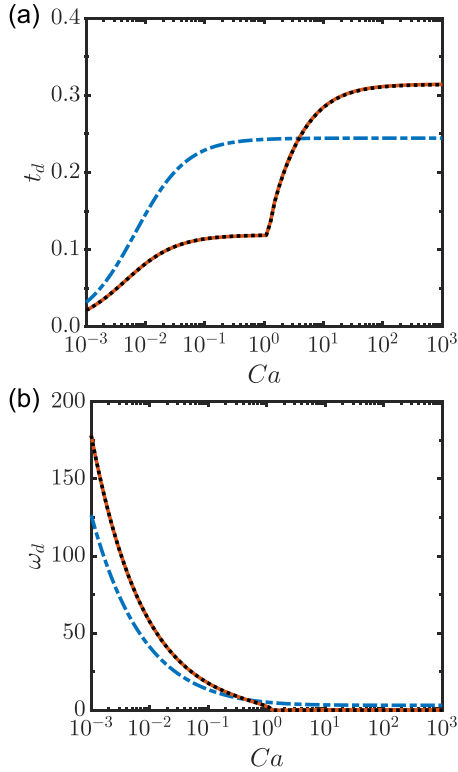
FIG. 8. (Color online) Dependence of the time constant (top) and damped natural frequency (bottom) on the Cauchy number for Flynn collapse based on linear analysis using the polytropic (dashed-dotted blue), heat transfer only (solid red), and heat/mass transfer (dotted black) models ($R_o/R_e = 2.09$ for the polytropic model, $R_o/R_e = 2.97$ with full thermal effects). Results presented in dimensionless form.

diagnostic and therapeutic ultrasound were investigated. Energy transport inside and outside the bubble is included in the numerical model, as well as the diffusion of vapor and non-condensible gas inside the bubble, assuming equilibrium phase change at the bubble wall. The soft material is described by a Kelvin-Voigt constitutive model with neo-Hookean (nonlinear) elasticity, appropriate for the finite deformations produced by large-amplitude bubble oscillations. A finite difference scheme was implemented to solve the PDEs for heat and mass transfer. Two collapse problems were considered: the classical Rayleigh and out-of-
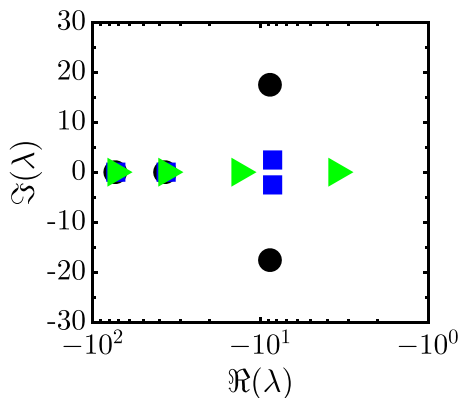

FIG. 9. (Color online) Eigenvalue map for Flynn collapse ($R_o/R_e = 2.97$ with full thermal effects), with Ca = 0.1 (black circle), 1.0 (blue square), and 10 (green triangle). Results presented in dimensionless form.
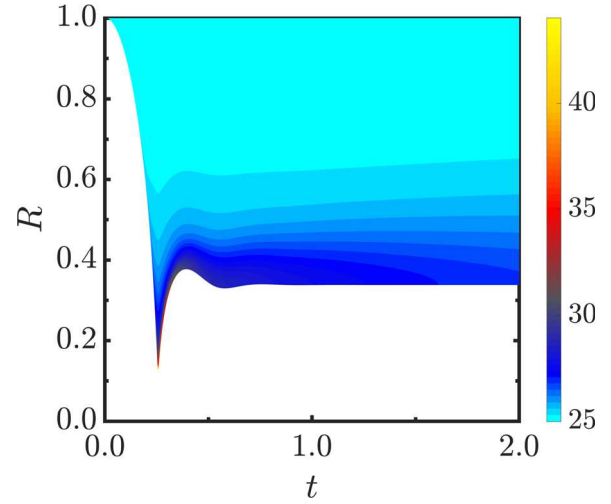

FIG. 10. (Color online) Temperature distribution in the surroundings for Flynn collapse ($R_o/R_e = 2.97$, Ca = 0.1). Results presented in dimensionless form, except for temperature (degrees Celsius).

equilibrium Flynn collapse problems. Small-amplitude (linear) perturbation analysis was used to explain the oscillatory behavior as the tissue stiffness is varied. We quantified the extent to which heat and mass transfer influence bubble dynamics depending on the stiffness. For Rayleigh collapse, we discovered that heat transfer significantly changes the behavior of the time constant (i.e., damping) at large Cauchy numbers (low shear moduli) where small radii at collapse are achieved, thus, facilitating heat transfer. This finding is substantiated by considering the eigenvalues corresponding to these thermal effects, which becomes dominant at small shear moduli. For the Flynn collapse, thermal effects matter at all Cauchy numbers. The oscillations become overdamped beyond a critical Cauchy number; due to the problem setup, elasticity enhances the violence of the collapse as an initial stress acts on the bubble. We further identify regimes under which a polytropic relation describes the heat transfer to sufficient accuracy, thus, avoiding the complexity and computational expense associated with solving full PDEs. This model provides a starting point for investigating the relative importance of thermal vs mechanical effects in ultrasound procedures. However, more accurate constitutive models and tissue characterization are required to make progress in this field.

ACKNOWLEDGMENTS

APPENDIX A

1. Convergence of the numerical scheme

The convergence of the numerical scheme is evaluated by considering the peak wall temperature and minimum bubble radius produced during Rayleigh collapse. The L_∞ errors

Carlos Barajas and Eric Johnsen

in these quantities in both the interior and exterior calculations are shown as a function of number of points in Fig. 11. The "exact" solution is taken as the solution obtained with $N_x = N_y = 1000$; the convergence of the interior scheme is evaluated holding $N_x = 1000$ while varying N_y, and vice versa for the exterior scheme. The L_∞ error is the difference between the "exact" and numerical solutions at the relevant time. As expected, the overall convergence rate is close to second order. The non-monotonic behavior observed in the interior solution is due to the change in direction of the root-finding algorithm for T_w. Additionally, we tracked the mass of non-condensible gas during our simulations,

$$M_{air} = 3R^3 \int_0^1 \rho_m (1 - C) y^2 \, dy. \tag{A1}$$

Although this value should remain constant throughout the simulation, the discretization errors compound to produce small deviations. However, no noticeable differences are observed in the bubble dynamics when the deviation is <5%.

2. Validity of the linear analysis

We compare in Fig. 12 results with linear analysis to those with our numerical solution of the full PDE model with heat and mass transfer, for Rayleigh collapse with Ca = 0.03. The excellent agreement supports the use of
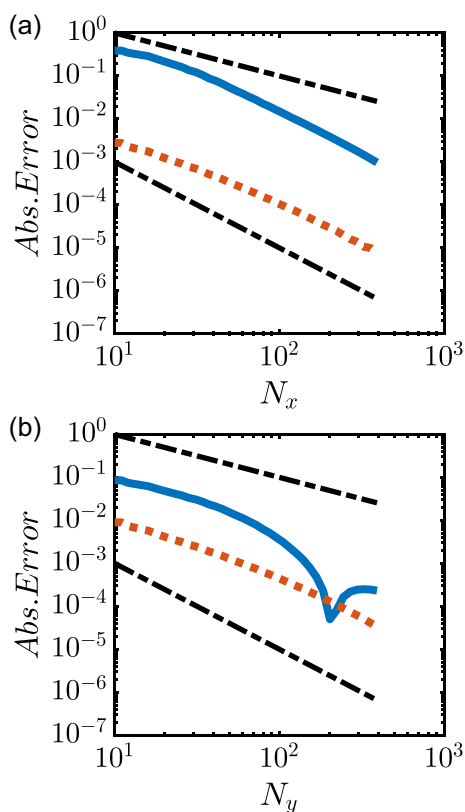

FIG. 11. (Color online) L_∞ error in peak temperature at the bubble wall T_w (solid blue) and minimum bubble radius (dotted red) for a typical Rayleigh collapse problem as the number of points in the bubble and medium are varied. The dashed-dotted lines denote $O(N)$ and $O(N^2)$. (Top) Interior ($N_y = 1000$), (Bottom) exterior ($N_x = 1000$).
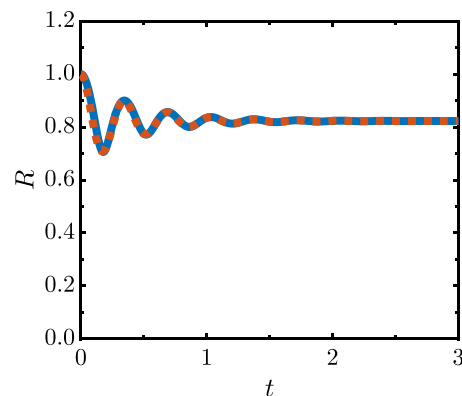

FIG. 12. (Color online) Time evolution of the bubble radius for the classical Rayleigh collapse problem ($\Delta p = 35 p_\infty$) with Ca = 0.03 (solid blue: full PDE model; red dotted: linearized solution). Results presented in dimensionless form.

linear analysis to explain our findings. For larger oscillation amplitudes, additional higher-order terms are required to accurately represent the solution;[38] however, linear analysis provides a qualitative description of the dominating physics.

[1]C. E. Brennen, *Cavitation and Bubble Dynamics* (Oxford University Press, Oxford, 1977), pp. 1–294.
[2]J. P. Franc and J. M. Michel, *Fundamentals of Cavitation* (Kluwer Academic, Dordrecht, 2004), pp. 1–306.
[3]T. G. Leighton, "Bubble population phenomena in acoustic cavitation," Ultrason. Sonochem. **2**, S123–S136 (1995).
[4]C. C. Coussios and R. A. Roy, "Applications of acoustics and cavitation to noninvasive therapy and drug delivery," Annu. Rev. Fluid Mech. **40**, 395–420 (2008).
[5]B. B. Goldberg, J. B. Liu, and F. Forsberg, "Ultrasound contrast agents: A review," Ultrasound Med. Biol. **20**, 319–333 (1994).
[6]J. E. Lingeman, "Extracorporeal shock wave lithotripsy. Development, instrumentation, and current status," Urol. Clin. North Am. **24**, 185–211 (1997).
[7]M. R. Bailey, V. A. Khokhlova, O. A. Sapozhnikov, S. G. Kargl, and L. A. Crum, "Physical mechanisms of the therapeutic effect of ultrasound (a review)," Acoust. Phys. **49**, 369–388 (2003).
[8]W. Roberts, T. L. Hall, K. Ives, J. S. Wolf, J. B. Fowlkes, and C. A. Cain, "Pulsed cavitational ultrasound: A noninvasive technology for controlled tissue ablation (histotripsy) in the rabbit kidney," J. Urol. **175**, 734–738 (2006).
[9]D. Dalecki, "Mechanical bioeffects of ultrasound," Annu. Rev. Biomed. Eng. **6**, 229–248 (2004).
[10]D. L. Miller, M. A. Averkiou, A. A. Brayman, E. C. Everbach, C. K. Holland, J. H. Wible, Jr., and J. Wu, "Bioeffects considerations for diagnostic ultrasound contrast agents," J. Ultrasound Med. **27**, 611–632 (2008).
[11]T. Y. Wang, Z. Xu, T. L. Hall, J. B. Fowlkes, and C. A. Cain, "An efficient treatment strategy for histotripsy by removing cavitation memory," Ultrasound Med. Biol. **38**, 753–766 (2012).
[12]L. Rayleigh VIII, "On the pressure developed in a liquid during the collapse of a spherical cavity," Philos. Mag. **34**, 94–98 (1917).
[13]M. S. Plesset, "The dynamics of cavitation bubbles," J. Appl. Mech. **16**, 277–282 (1949).
[14]M. S. Plesset and A. Prosperetti, "Bubble dynamics and cavitation," Annu. Rev. Fluid Mech. **9**, 145–185 (1977).
[15]A. Prosperetti, L. A. Crum, and K. W. Commander, "Nonlinear bubble dynamics," J. Acoust. Soc. Am. **83**, 502–514 (1988).
[16]V. Kamath, A. Prosperetti, and F. N. Egolfopoulos, "A theoretical study of sonoluminescence," J. Acoust. Soc. Am. **94**, 248–260 (1993).
[17]L. Stricker, A. Prosperetti, and D. Lohse, "Validation of an approximate model for the thermal behavior in acoustically driven bubbles," J. Acoust. Soc. Am. **130**, 3243–3251 (2011).
[18]W. Lauterborn, "Numerical investigation of nonlinear oscillations of gas bubbles in liquids," J. Acoust. Soc. Am. **59**, 283–293 (1976).

J. Acoust. Soc. Am. **141** (2), February 2017

Carlos Barajas and Eric Johnsen   917

[19]S. Fujikawa and T. Akamatsu, "Effects of the non-equilibrium condensation of vapour on the pressure wave produced by the collapse of a bubble in a liquid," J. Fluid Mech. **97**, 481–512 (1980).

[20]B. D. Storey and A. J. Szeri, "Water vapour, sonoluminescence and sonochemistry," Proc. R. Soc. A Math. Phys. Eng. Sci. **456**, 1685–1709 (2000).

[21]R. I. Nigmatulin, N. S. Khabeev, and F. B. Nagiev, "Dynamics, heat and mass transfer of vapour-gas bubbles in a liquid," Int. J. Heat Mass Transf. **24**, 1033–1044 (1981).

[22]W. Kreider, "Gas-vapor bubble dynamics in therapeutic ultrasound," Ph.D. thesis, University of Washington, 2008.

[23]W. Kreider, L. A. Crum, and M. R. Bailey, "A reduced-order, single-bubble cavitation model with applications to therapeutic ultrasound," J. Acoust. Soc. Am. **130**, 3511–3530 (2011).

[24]A. T. Preston, "Modeling heat and mass transfer in bubbly cavitating flows and shock waves in cavitating nozzles," Ph.D. thesis, California Institute of Technology, 2004.

[25]I. Akhatov, O. Lindau, A. Topolnikov, R. Mettin, N. Vakhitova, and W. Lauterborn, "Collapse and rebound of a laser-induced cavitation bubble," Phys. Fluids **13**, 2805–2819 (2001).

[26]A. Preston, T. Colonius, and C. E. Brennen, "A reduced-order model of diffusive effects on the dynamics of bubbles," Phys. Fluids **19**, 123302 (2007).

[27]K. Ando, "Effects of polydispersity in bubbly flows," Ph.D. thesis, California Institute of Technology, 2010.

[28]K. Ando, T. Colonius, and C. E. Brennen, "Numerical simulation of shock propagation in a polydisperse bubbly liquid," Int. J. Multiphase Flow **37**, 596–608 (2011).

[29]H. S. Fogler and J. D. Goddard, "Collapse of spherical cavities in viscoelastic fluids," Phys. Fluids **13**, 1135–1141 (1970).

[30]I. Tanasawa, "Dynamic behavior of a gas bubble in viscoelastic liquids," J. Appl. Phys. **41**, 4526–4531 (1970).

[31]R. Y. Ting, "Viscoelastic effect of polymers on single bubble dynamics," AIChE J. **21**, 810–813 (1975).

[32]J. S. Allen and R. A. Roy, "Dynamics of gas bubbles in viscoelastic fluids. I. Nonlinear viscoelasticity," J. Acoust. Soc. Am. **107**, 3167–3178 (2000).

[33]J. S. Allen and R. A. Roy, "Dynamics of gas bubbles in viscoelastic fluids. II. Nonlinear viscoelasticity," J. Acoust. Soc. Am. **108**, 1640–1650 (2000).

[34]J. Jimenez-Fernandez and A. Crespo, "Bubble oscillation and inertial cavitation in viscoelastic fluids," Ultrasonics **43**, 643–651 (2005).

[35]J. Naude and F. Mendez, "Periodic and chaotic acoustic oscillations of a bubble gas immersed in an upper convective Maxwell fluid," J. Non-Newton. Fluid Mech. **155**, 30–38 (2008).

[36]X. Yang and C. C. Church, "A model for the dynamics of gas bubbles in soft tissue," J. Acoust. Soc. Am. **118**, 3595–3606 (2005).

[37]R. Gaudron, M. T. Warnez, and E. Johnsen, "Bubble dynamics in a viscoelastic medium with nonlinear elasticity," J. Fluid Mech. **766**, 54–75 (2015).

[38]C. Hua and E. Johnsen, "Nonlinear oscillations following the Rayleigh collapse of a gas bubble in a linear viscoelastic (tissue-like) medium," Phys. Fluids **25**, 083101 (2013).

[39]M. T. Warnez and E. Johnsen, "Numerical modeling of bubble dynamics in viscoelastic media with relaxation," Phys. Fluids **27**, 063103 (2015).

[40]J. Keller and M. Miksis, "Bubble oscillations of large amplitude," J. Acoust. Soc. Am. **68**, 628–633 (1980).

[41]A. Prosperetti, "The thermal behaviour of oscillating gas bubbles," J. Fluid Mech. **222**, 587–616 (1991).

[42]L. A. Crum, "Measurements of the growth of air bubbles by rectified diffusion," J. Acoust. Soc. Am. **68**, 203–211 (1980).

[43]F. Hamaguchi and K. Ando, "Linear oscillation of gas bubbles in a viscoelastic material under ultrasound irradiation," Phys. Fluids **27**, 113103 (2015).

[44]P. N. T. Wells and H.-D. Liang, "Medical ultrasound: Imaging of soft tissue strain and elasticity," J. R. Soc. Interface **8**, 1521–1549 (2011).

[45]P. J. Prince and J. R. Dormand, "High order embedded Runge-Kutta formulae," J. Comput. Appl. Math. **7**, 67–75 (1981).

[46]R. P. Brent, "An algorithm with guaranteed convergence for finding a zero of a function," Comput. J. **14**, 422–425 (1971).

[47]H. G. Flynn, "Cavitation dynamics. I. A mathematical formulation," J. Acoust. Soc. Am. **57**, 1379–1396 (1975).

[48]H. G. Flynn, "Cavitation dynamics: II. Free pulsations and models for cavitation bubbles," J. Acoust. Soc. Am. **58**, 1160–1170 (1975).